

Modelling and Testing of an Ultra-low Temperature sCO₂ Opposing Piston Heat Engine

Joshua Schmitt
Research Engineer
Southwest Research Institute
San Antonio, Texas
Phone: 210-522-6777
joshua.schmitt@swri.org

Jordan Nielson
Research Engineer
Southwest Research Institute
San Antonio, Texas
Phone: 210-522-2143
jordan.nielson@swri.org

Nathan Poerner
Senior Research Engineer
Southwest Research Institute
San Antonio, Texas
Phone: 210-522-6584
nathan.poerner@swri.org



Joshua Schmitt is a Research Engineer at Southwest Research Institute. He has performed extensive research into supercritical CO₂ systems and components, including for his graduate thesis. He has performed cost of electricity analysis and machinery design for solar-thermal sCO₂ systems for DOE projects. He is the project manager for several multi-million dollar DOE projects for oxy-combustion power cycles.



Jordan Nielson is a Research Engineer at Southwest Research Institute. Mr. Nielson designs flow loops, gathers data, and post processes data for testing customer flow components. Mr. Nielson conducted testing of leak detection systems for pipelines undergoing two-phased slug flow. He provides mechanical design expertise, engineering support, and project management oversight for a wide variety of projects related to testing fluid systems in the Fluid Dynamics Section.



Nathan Poerner is a Senior Research Engineer at Southwest Research Institute. Mr. Poerner has extensive experience in the areas of high-speed data acquisition and control systems, measuring dynamic pressure pulsations, measuring dynamic strain and measuring vibration (both lateral and torsional). He is also proficient with impact/modal testing and Operating Deflection Shape (ODS) analyses. Additionally, he has experience with compressor performance testing.

ABSTRACT

Southwest Research Institute (SwRI,) along with Thermal Tech Holdings, LLC, has modeled, built, and tested a heat engine that generates power from ultra-low temperature heat sources. The CO₂ was designed to be contained within a heat exchanger and piston cylinder volume and pressurized to supercritical pressures. The cycle was developed based on the expansive properties of sCO₂, and it can produce power even at temperatures as low as 130°F. An engine was conceptualized that uses opposing motion to expand and compress CO₂ with ultra-low temperature heat sources. A time-dependent model was programmed in Matlab that demonstrates how the CO₂ builds pressure with temperature and changes properties with volume. This model helped select the sizing of the engine for a demonstration test of the novel technology at the 10kWe scale, producing power by pumping hydraulic oil to a hydraulic motor. The engine was assembled at SwRI for testing. During the testing, a wide range of flows and temperatures of water were used to characterize the performance of the engine. The results of the testing and their implications are discussed.

NOMENCLATURE

a	Acceleration
A	Area
ρ	Density
d	Diameter
μ	Dynamic Viscosity
η	Efficiency
h	Enthalpy
s	Entropy
f	Friction Factor
Q	Heat Energy
PR	Hydraulic to CO2 Pressure Ratio
m	Mass
D	Motor Displacement
x	Position
P	Pressure
Re	Reynolds Number
N	Rotational Speed
ϵ	Surface Roughness
T	Temperature
t	Time
v	Velocity
V	Volume
W	Work Energy

INTRODUCTION

In late of 2016, SwRI was contracted by Thermal Tech Holdings, LLC to conduct research into a novel piston engine capable of producing power from ultra-low temperature heat sources. The resulting engine concept is based on the fundamental characteristics of the thermal expansion of CO₂ near the critical point (sCO₂), although it could be used with other working fluids. SwRI proceeded through a conceptualization, modelling, design, layout (Figure 1), assembly, and testing of the engine.

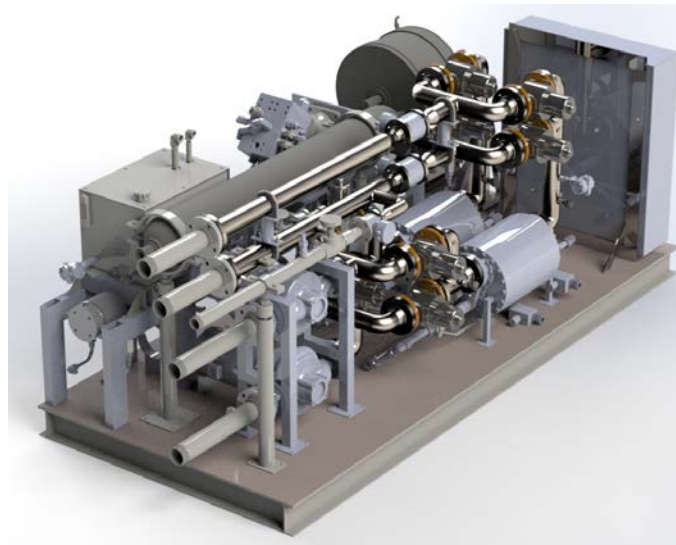


Figure 1. 3D Layout of the Ultra-Low Temperature Heat Engine

The first engine was designed to be tested and then shipped to a geothermal resource in northern California where the heat source is a hot geothermal well that has a water temperature of approximately 190°F

CYCLE CONCEPT

The thermal expansion of sCO₂, depending on its specific volume, can create significantly high pressures that can drive expansion. For example, if the CO₂ in its most compact state is at 90°F and 35.83 in³/lbm, for the same volume it will go from 1600 psi to 3000 psi for a temperature increase to 128.3°F. This high pressure can be leveraged to produce power and drive compression of CO₂ in an opposing piston arrangement, as shown in Figure 2.

The concept was developed on the basic premise that the sCO₂ would act as an intermediary working fluid that is trapped between a heat exchanger and a piston cylinder volume. This premise requires that the heat source be cyclically alternated on the same heat exchanger, with heating being supplied during expansion, and cooling being supplied during compression.

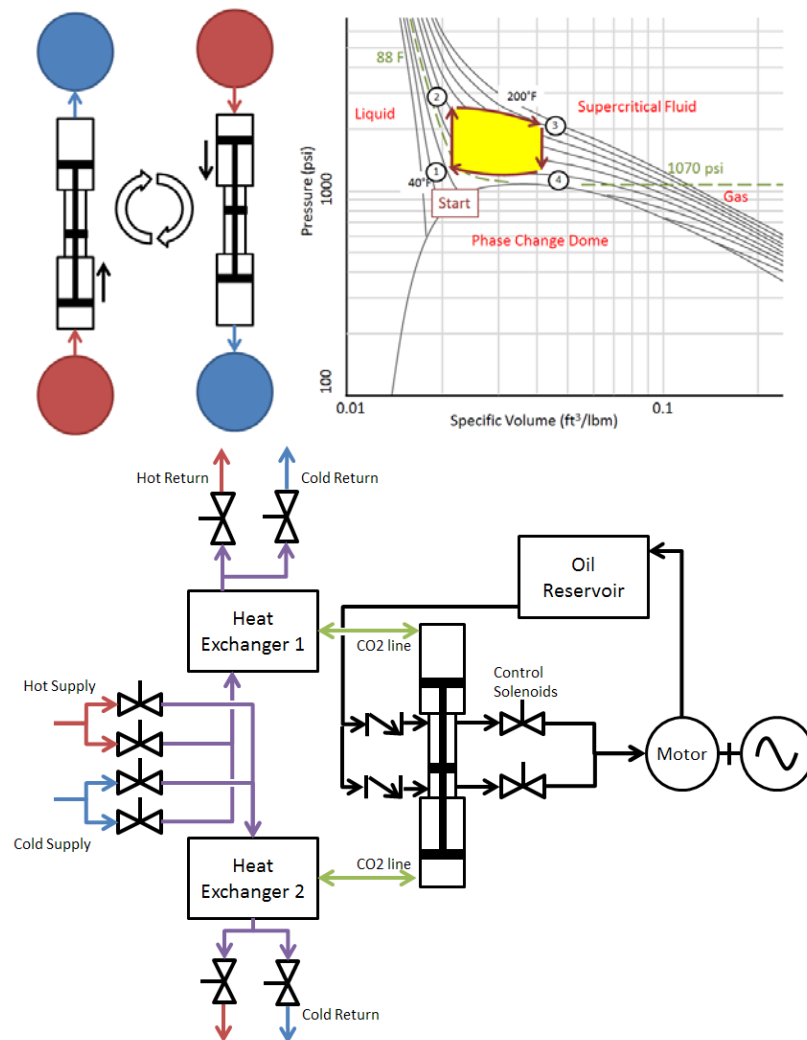


Figure 2. Opposing Piston Concept with Cycling Heat Sources and Cycle Overlaid on a CO₂ P-V Diagram and an Example Block Diagram

The fundamental cycle is also shown in Figure 2 on a pressure versus volume basis. Thermodynamics tells us that the work output of the cycle is dependent on the yellow highlighted area of the cycle. The cycle maximum pressure is limited by material strength and pressure rating of the various components. Figure 2 also demonstrates how valves control the flow of heat to each heat exchanger. It also shows the concept of control solenoids, which prevent the piston from moving, and, when open, supply the motor with pressurized oil.

The cycle begins in the most compressed state at the coldest temperature, which is state 1. If the cycle was then allowed to expand with a natural balance of forces, the expansion would happen at low temperature and the cycle would not produce much power. To improve power, state point 1 to 2 holds the cycle at a minimum volume, adds heat to the fluid, and waits until a pre-determined safe release point for expansion. This maximum pressure at minimum volume is state point 2. Between state points 2 and 3 is the expansion of the cylinder, which also includes additional heating from the heat exchanger to improve the final temperature of the expanded CO₂. State point 3 is the maximum volume and hottest temperature condition. From state point 3 to state point 4, the piston is held at maximum volume and cooled over the same amount of time as the heating from state 1 to 2. Thus, state point 4 is the point of pressure at maximum volume before expansion begins. From state point 4 to state point 1, the CO₂ is cooled and compressed.

MODELLING

Since power output is dependent on the highlighted area in the engine cycle, the estimated work is dependent on the path the pressure takes during expansion and compression. Thus, time-dependent modelling is needed to understand the power output of the proposed cycle. The basic premise of the opposing piston motion with its balance of forces is shown in Figure 3. The force balance model uses the different surface areas and pressures along with seal friction to predict the piston movement.

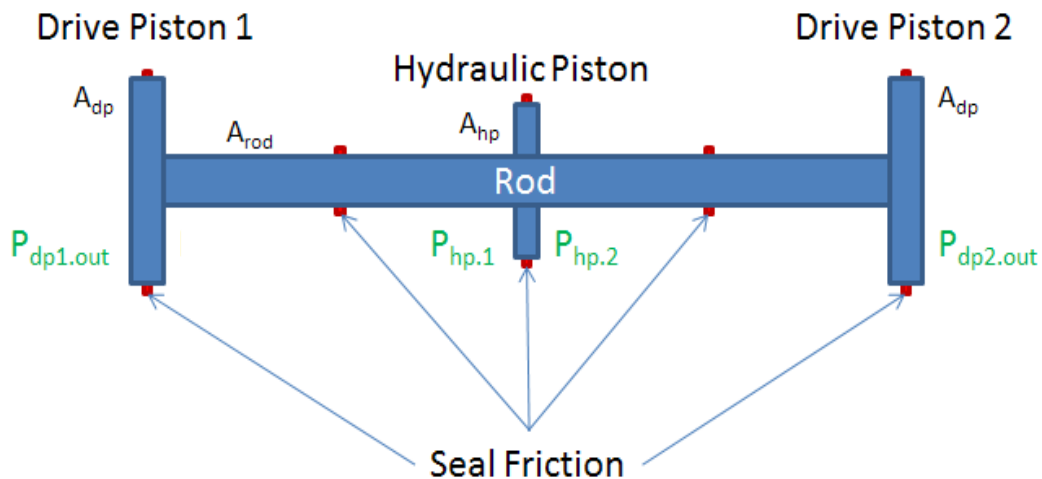


Figure 3. Opposing Piston Pressure Balance Model Basis

The equations governing piston movement are shown in Equation 1. From this piston position, speed, and acceleration can be tracked. A preliminary representation of this effect was modelled in Excel using REFPROP [1] lookup functions to find CO₂ state properties. The Excel model was only partially time dependent, as it was only looking at the potential balance of forces, position, velocity, and acceleration of the pistons.

Equation 1

$$m * a = \sum P * A - \sum F_{friction}$$

$$\Delta v = a * dt$$

$$\Delta x = v_o * dt + 0.5 * a * dt^2$$

The Excel model calculated position change with a 10 millisecond time step. It provided pressures and temperatures of CO2 in the system, assuming that the heat addition of the heat exchanger was distributed evenly throughout the system. The heat exchanger volumes and heat transfers were varied to help provide guidance as to the design of the heat exchangers for the test. An example result of the modelling in Excel is shown in Figure 4.

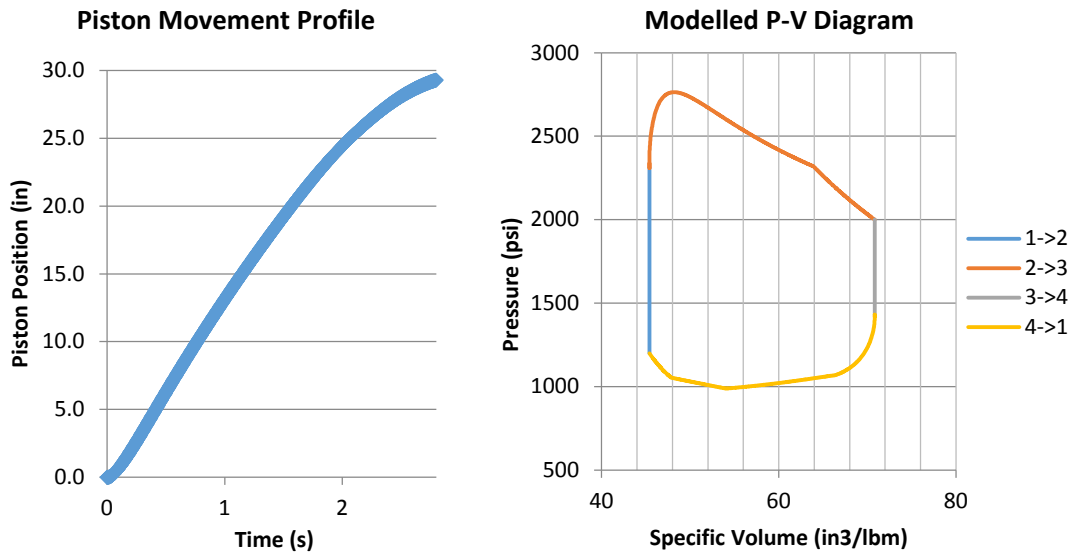


Figure 4. Preliminary Model Piston Profile and P-V Diagram

The estimates of performance and underlying equations were used to build a more completely time-dependent model in Matlab, again referencing equation of state values from REFPROP [1].

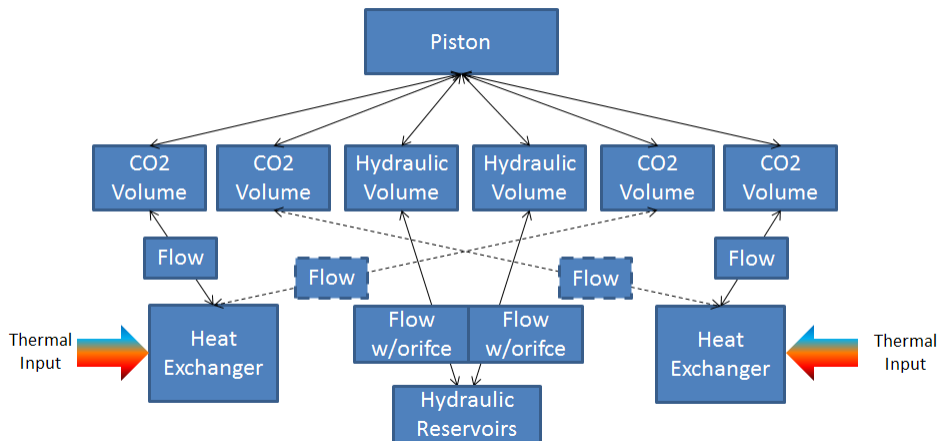


Figure 5. Control Volume Based Fully Time-Dependent Model

Since the target time step for this model was 5 milliseconds, the REFPROP CO2 state points were brought into a lookup table that ranged from 20°F to 400°F with pressures from 500 to 5000 psi to improve computation times. These ranges were evenly divided into 1000 points of table data for density, enthalpy, entropy, and other necessary fluid properties. The Matlab model used a control volume approach which is shown in Figure 5.

The Matlab model tracked changes in control volume size, CO2 properties, fluid mass transfer, heat transfer, pressure loss, heat loss, and other critical effects on the cycle performance. Figure 6 shows the control volume approach to transferring heat from a water input through metal to the CO2 contained in the heat exchanger. This CO2 can also leave or enter the heat exchanger as a mass flow based on an imbalance of pressure due to properties changing or piston movement.

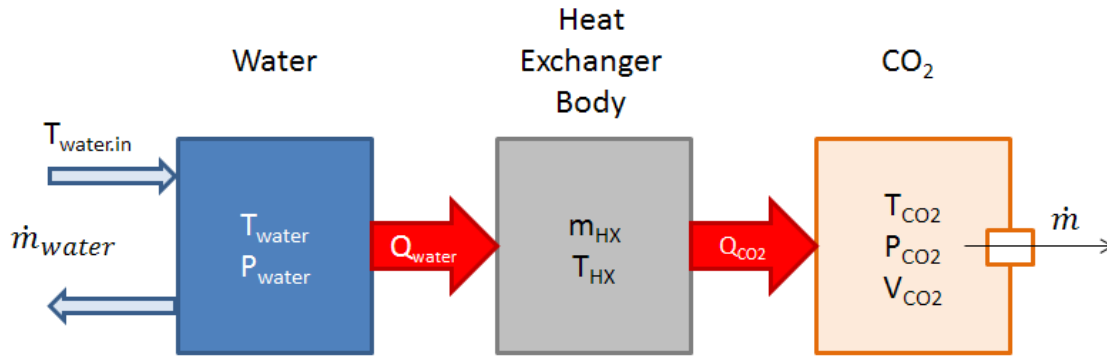


Figure 6. Heat Exchanger Control Volume Method of Heat and Mass Transfer

The governing equations on the heat transfer on the heat exchangers are shown in Equation 2. The change in properties of the CO2 and water are tracked based on heat and mass transfer and the referencing of the CO2 state lookup tables. The heat transfer is estimated on an average CO2 temperature basis where the temperature throughout the heat exchanger is assumed to be an average value compared to the changing water temperature as it leaves and enters along the length of the heat exchanger. A volume of water is tracked from entrance to exit of the heat exchanger as the equation solves relative to its changing temperature and the changing average CO2 temperature.

Equation 2

$$\Delta H_{water} = \dot{m}_{water} * (h_{water.in} - h_{water}) * dt - Q_{water}$$

$$T_{water} = \text{Temperature}(P_{water}, h_{water})$$

$$Q_{water} = h_{water} * A_{water} * (T_{water} - T_{HX}) * dt$$

$$P_{cyl} = \text{Pressure}(T_{cyl}, \rho_{CO2})$$

$$T_{cyl} = \text{Temperature}(h_{CO2}, \rho_{CO2})$$

$$Q_{CO2} = h_{CO2} * A_{CO2} * (T_{HX} - T_{CO2})$$

$$\Delta H_{CO2} = Q_{CO2} - \dot{m} * h_{CO2} * dt$$

$$\Delta T_{HX} = \frac{Q_{water} - Q_{CO2}}{c_{HX} * m_{HX}}$$

The piston also behaves as a control volume with mass and heat transfer balance. However, heat is not

being actively added or removed. Instead, during moments of compression or expansion, the space in the cylinder changes in volume and the gas changes in density. The piston control volume, along with relevant heat, mass, and volume equations are shown in Figure 7.

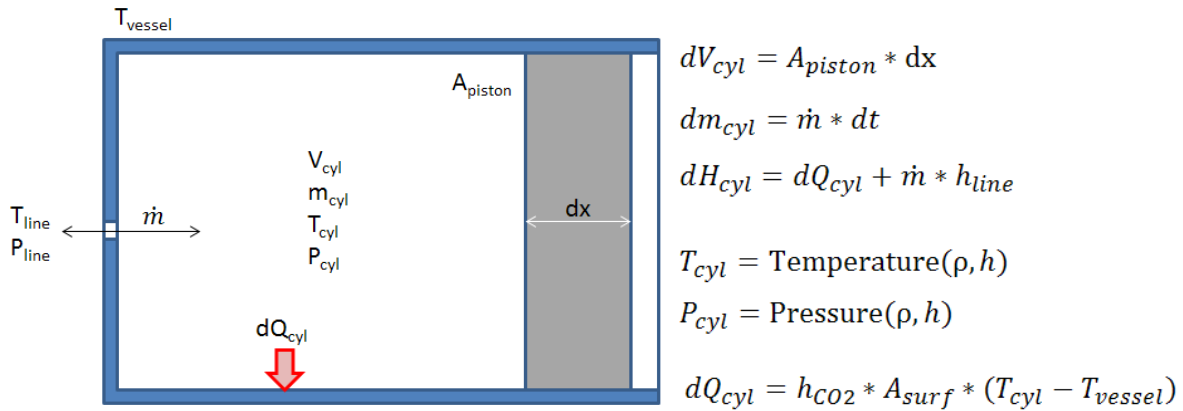


Figure 7. Piston Control Volume with Mass and Heat Transfer and Volume Change Equations

The equations governing the potential for mass to transfer between volumes on the CO2 and hydraulic side are shown in Equation 3. The difference in pressure will lead to a certain velocity of flow and, hence, a mass flow rate.

Equation 3

$$Re_d = \frac{\rho * v_{flow} * d}{\mu}$$

$$\frac{1}{f^{1/2}} = -2 * \log\left(\frac{\epsilon/d}{3.7} + \frac{2.51}{Re_d * f^{1/2}}\right)$$

$$\Delta P = \frac{1}{2} * \rho * f * v_{flow}^2$$

The Matlab model, after undergoing a few revisions, was capable of modeling a cycle that tracks the mass and heat change of the engine system. Figure 8 shows the modeled change in piston position and the corresponding pressure changes

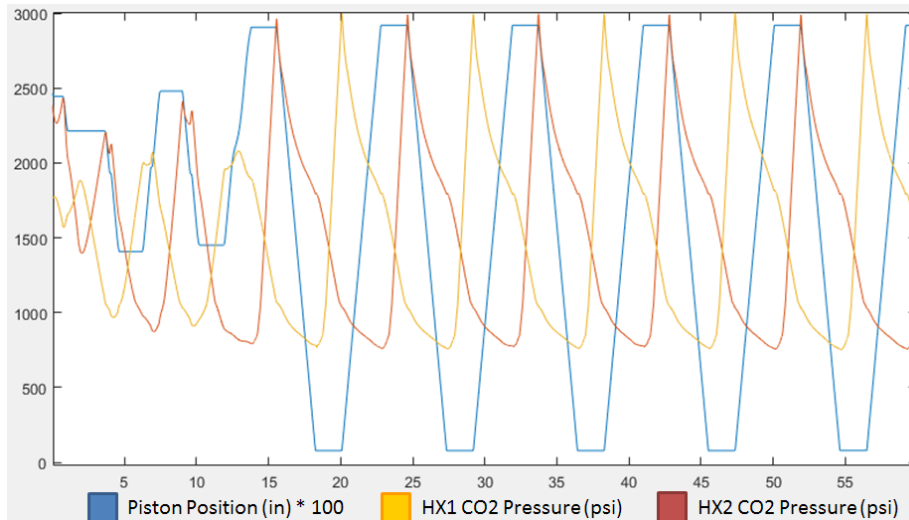


Figure 8. Example Matlab Model Result with Piston Position and CO2 Pressure Output

It is important to note that the model is unstable in the beginning of the run, but with the proper initialization and once it is properly stabilized, the piston falls into a cycling pattern. The results from the model shown includes controls that limit the speed of the piston to a maximum velocity, hence the constant slopes in piston movement. It was observed during earlier versions of the model that the quick speed of the engine near the start of the cycle would cause large losses in pressure and result in a cycle that produces very little power. Hence, the modelling, not only helped determine sizes of control volumes, but also methods of controlling the engine.

TEST SETUP

Figure 9 shows the assembled engine for testing at SwRI's test location in San Antonio, Texas.

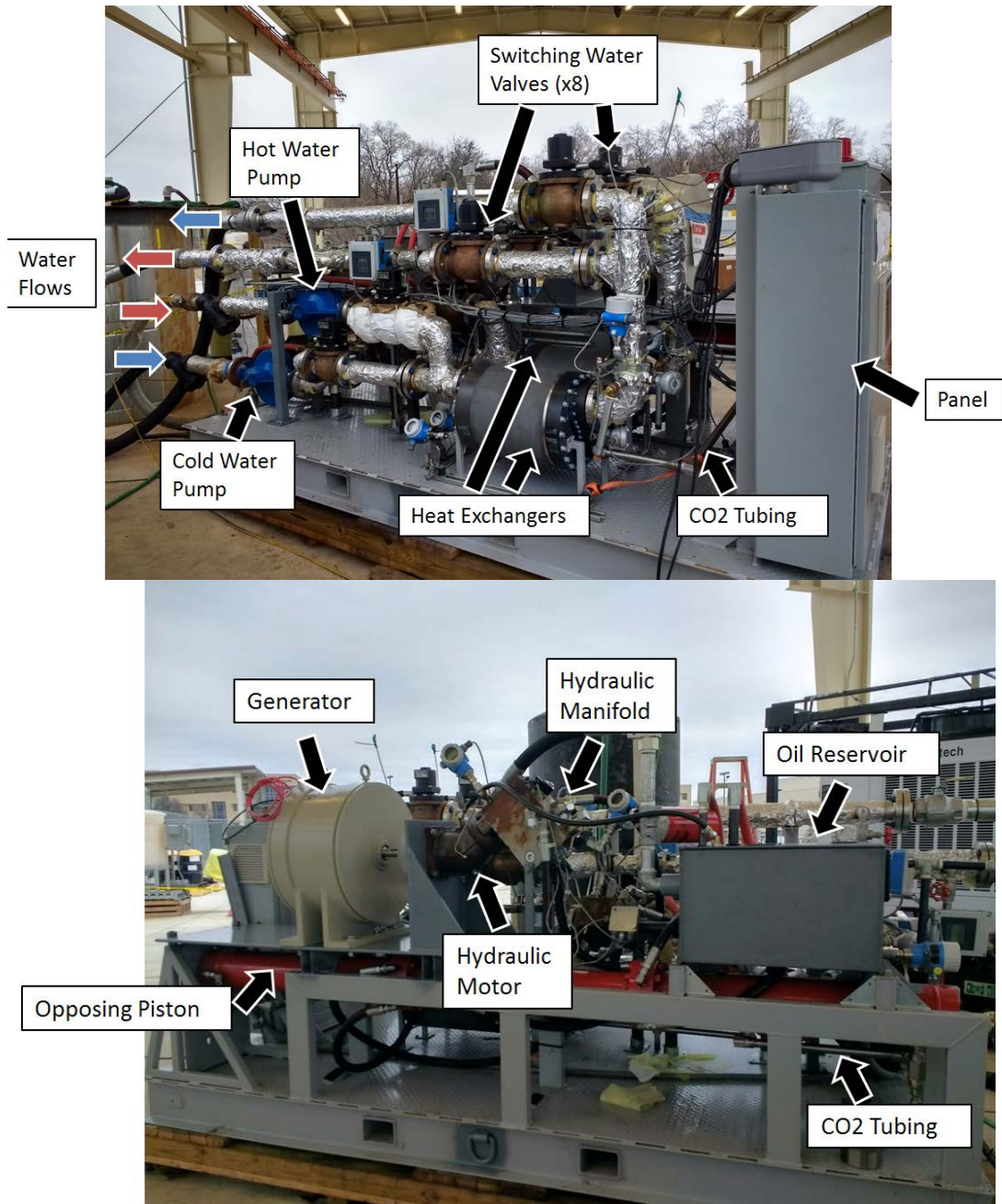


Figure 9. Side Views of the Assembled Engine with Major Components Labelled

The opposing piston cylinder has a stroke length of 30 inches. Piston position information is read from a MTS position sensor. Tubing connects the CO₂ from one end of the heat exchanger to the corresponding end of the piston cylinder. Water is delivered by 2 2HP pumps to the heat exchangers. Solenoid water valves combined with splits in the piping are used to control which water flow is directed to each heat exchanger and what temperature flows are being looped back to the hot and cold sources. The test was performed with 2 Watlow heaters with 175 kW of power output each. A 30 ton chiller was used to cool the return water to the desired temperature. Tanks over 1000 gallons were used to maintain an average temperature entering the hot and cold side.

The hydraulic piston cylinder was connected to a manifold block which connects directly to the hydraulic motor. The flow of oil controls the motion of the piston the level of control needed to generate more power in the cycle was achieved with hydraulic flow regulators and solenoid valves. An electric generator is attached to the hydraulic motor. At the intended installation, power is passed through a rectifier into an inverter to compensate for the wide variation in power output due to the stop-and-start operation of the motor.

The pressure ratio applied by the cylinder of hydraulic pressure to CO₂ pressure was approximately 2.2. For this test a volume ratio of approximately 1.8 of maximum volume to minimum volume was chosen as the design ratio.

TEST RESULTS AND DISCUSSION

Once the rig was commissioned at the test site, a series of tests were run based on the intended operation at a geothermal resource. A hot water inlet temperature of 190°F, a cold water inlet temperature of 45°F, and a water flow rate of approximately 80 GPM was chosen as the design point. An example set of test result data for the design conditions versus time is shown in Figure 10.

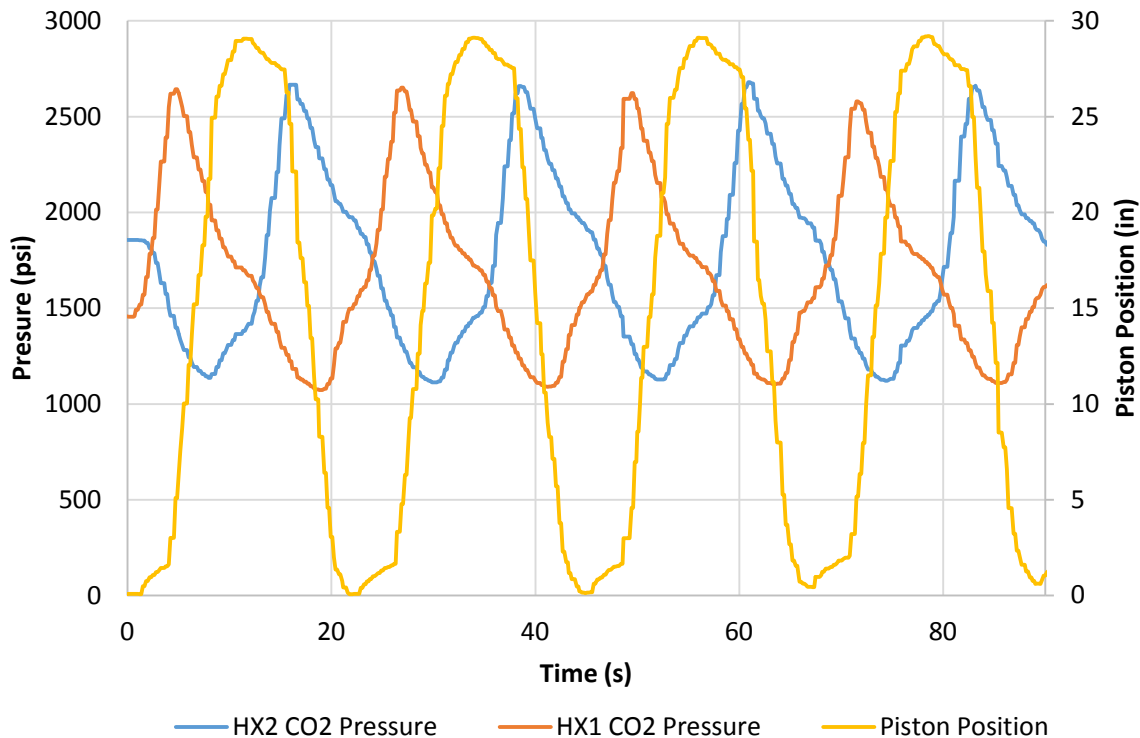


Figure 10. Test Data Showing CO₂ Pressures and Piston Position of the Engine at 190F Hot Water Temperature, 45F Cold Water Temperature, and Water Flow Rate of 80 GPM

The piston behaves similarly to the Matlab results in Figure 8, but with a longer overall cycle time. Thus, the speed of heat exchange and the speed of expansion should be adjusted in the Matlab model to better represent the test behavior. For the design condition a set of P-V and T-s diagrams were generated based on the known volume ratio and mass of CO₂ added to the system. These two cycle diagrams with recorded test data were overlaid on state diagrams from REFPROP [1] and shown in Figure 11.

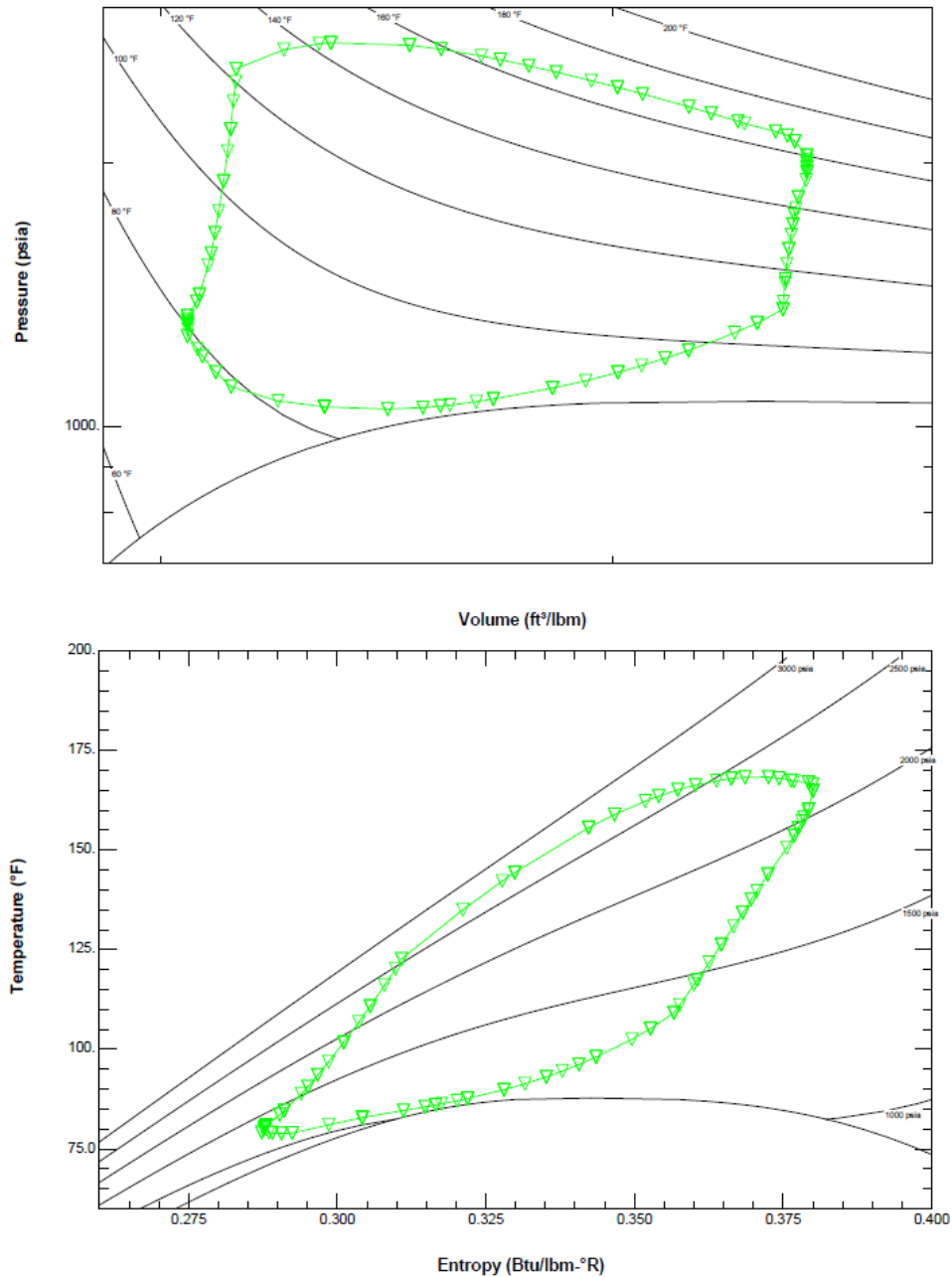


Figure 11. P-V and T-s Diagrams of the Engine at 190F Hot Water Temperature, 45F Cold Water Temperature, and Water Flow Rate of 80 GPM

The equation set for determining cycle power based on the P-V diagram is presented in Equation 4. The discretized path presented by the P-V diagram in Figure 11 is taken over the entire cycle on a stepwise

basis and summed for the available work, which is divided by the cycle time to compute power. Note that the pressure of expansion and compression is specified in the equation which changes depending on which heat exchanger is experiencing heating or cooling once the heat exchangers switch their input sources.

Equation 4

$$\dot{W}_{cycle} = \left[\int P_{exp}(V)dV - \int P_{comp}(V)dV \right] / dt_{cycle}$$

$$\dot{W}_{cycle} = \left[\sum_{i=Cycle\ Start}^{i=Cycle\ End} \frac{(P_{i,exp} + P_{i+1,exp})}{2} (V_{i+1} - V_i) - \frac{(P_{i,comp} + P_{i+1,comp})}{2} (V_{i+1} - V_i) \right] / dt_{cycle}$$

The heat input into the cycle can be similarly determined using the T-s diagram, as shown in Equation 5. The temperature and entropy can be used during the heating portion of the cycle to determine the heat flow rate. Again, the calculation changes depending on which body of CO₂ is experiencing heating once the heat exchangers switch from hot to cold. For both calculations, the sum is taken after a complete cycle, which equals two strokes of the opposing piston.

Equation 5

$$\dot{Q}_{H,cycle} = \left[\int T_{heating}(s)ds \right] / dt_{cycle}$$

$$\dot{Q}_{H,cycle} = \left[\sum_{i=Cycle\ Start}^{i=Cycle\ End} \frac{(T_{i,heating} + T_{i+1,heating})}{2} (s_{i+1} - s_i) \right] / dt_{cycle}$$

The tested engine is capable of measuring the shaft output power more directly. The shaft power of the motor is shown in Equation 6. The pressure drop across the motor is dependent on the oil pressure at the manifold before the motor. The rotational speed is read directly from a proximity sensor that measure the time between pulses. The hydraulic motor is a constant displacement type with a displacement of 179.8 cm³/rev. Equation 6 includes the necessary conversions of the displacement, rotational speed, and pressure, in psi, to calculate the power in kilowatts. The efficiency was taken to be approximately 95%.

If the installed hydraulic oil pressure sensor leading to the motor dropped below a certain pressure, it would appear to delay in reading the actual pressure of the oil. This delay occurred after the piston is released during the critical, high-pressure beginning of the stroke. When checked against the calculated pressure in oil based on CO₂ pressure readings, shown in Equation 7, the hydraulic pressure sensor followed calculated trends closely after nearly 50% of the stroke had been completed. Given that the oil is assumed to be mostly incompressible, the oil could not be compressing over more than 50% of the piston stroke. Furthermore, the CO₂ pressure sensors responded quickly because they never experienced a loss in pressure. Based on tests for certain hydraulic oil flow rates when the hydraulic oil pressure sensor followed expected trends, a dynamic pressure loss of approximately 250 psi on average was observed. Thus, the calculation of motor shaft power uses the CO₂ pressure readings with the dynamic pressure loss and the proximity sensor for RPM.

Equation 6

$$\dot{W}_{shaft} = \frac{N * D * \Delta P * \eta_{mech}}{60 * 8.8507 * 1000 * 2.54}$$

Equation 7

$$\Delta P = |P_{CO2,HX1} - P_{CO2,HX2}| PR_{static} - P_{loss,dynamic} - P_{atm}$$

Equation 8

$$\eta_{th,cycle} = \frac{\dot{W}}{\dot{Q}_H}$$

When calculating efficiency of the cycle, Equation 8 is used. The efficiency and power values for a range of off-design not inlet temperatures are shown in Figure 12. The motor shaft power is on average 90.1% less than the cycle power taken from the P-V diagram. The cycle efficiencies use the heat and power calculated from the T-s and P-v diagrams for each recorded run.

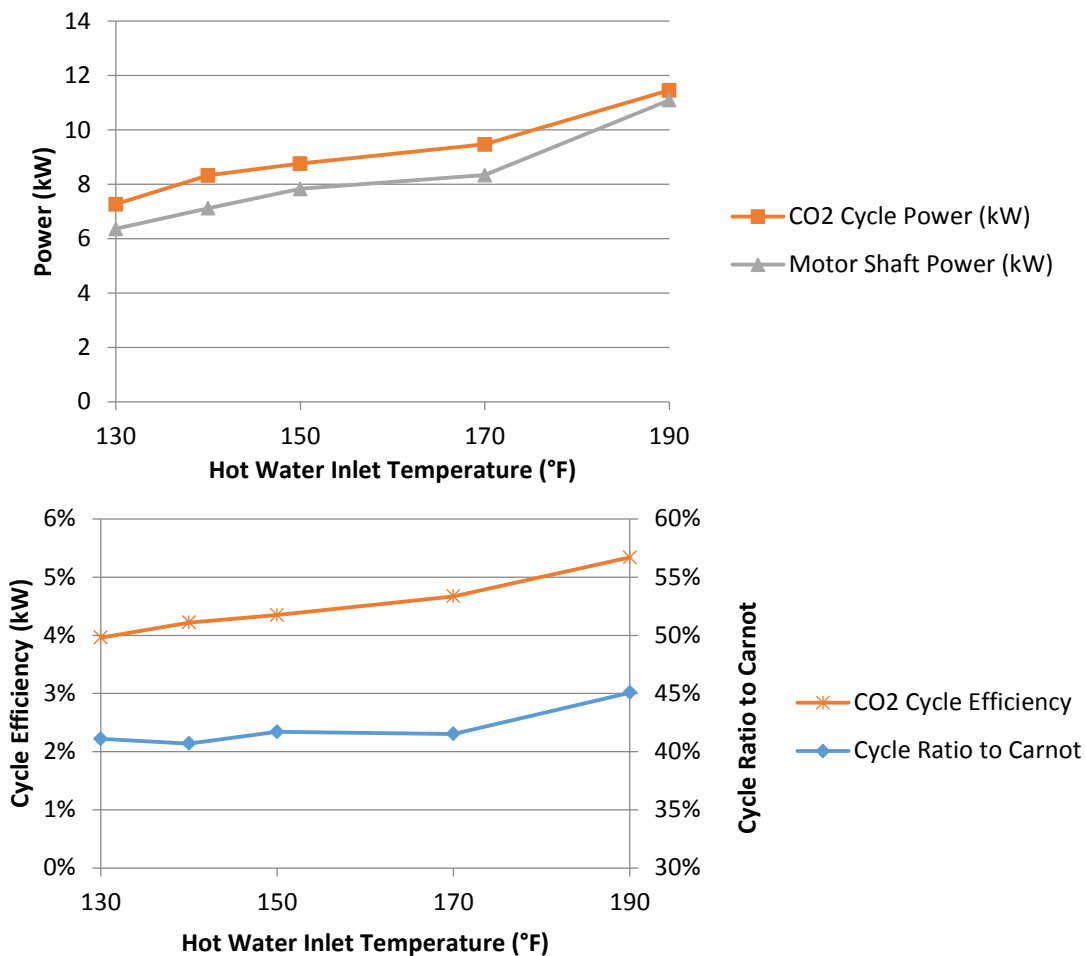


Figure 12. Effect on Power Output and Efficiency with Changes in Hot Water Temperature for 45F Cold Water Temperature and Water Flow Rate of 80 GPM

A comparison of these cycle efficiencies to the theoretical Carnot cycle is also shown. This references a Carnot cycle that uses the maximum and minimum temperatures and entropies in the cycle. Since the theoretical maximum thermal efficiency is low at these temperatures, a ratio to Carnot often provides a better mechanism for comparing the cycle's performance to its maximum potential.

Off-design power and efficiency for increasing cold inlet temperature and decreasing water flow rate are shown in Figure 13. The trends indicate that decreasing the gap between hot and cold flow temperatures will reduce power, which follows the principles of a heat engine. Decreasing water flow also impacts power output and efficiency because not enough heat is available to operate at the maximum power and efficiency condition.

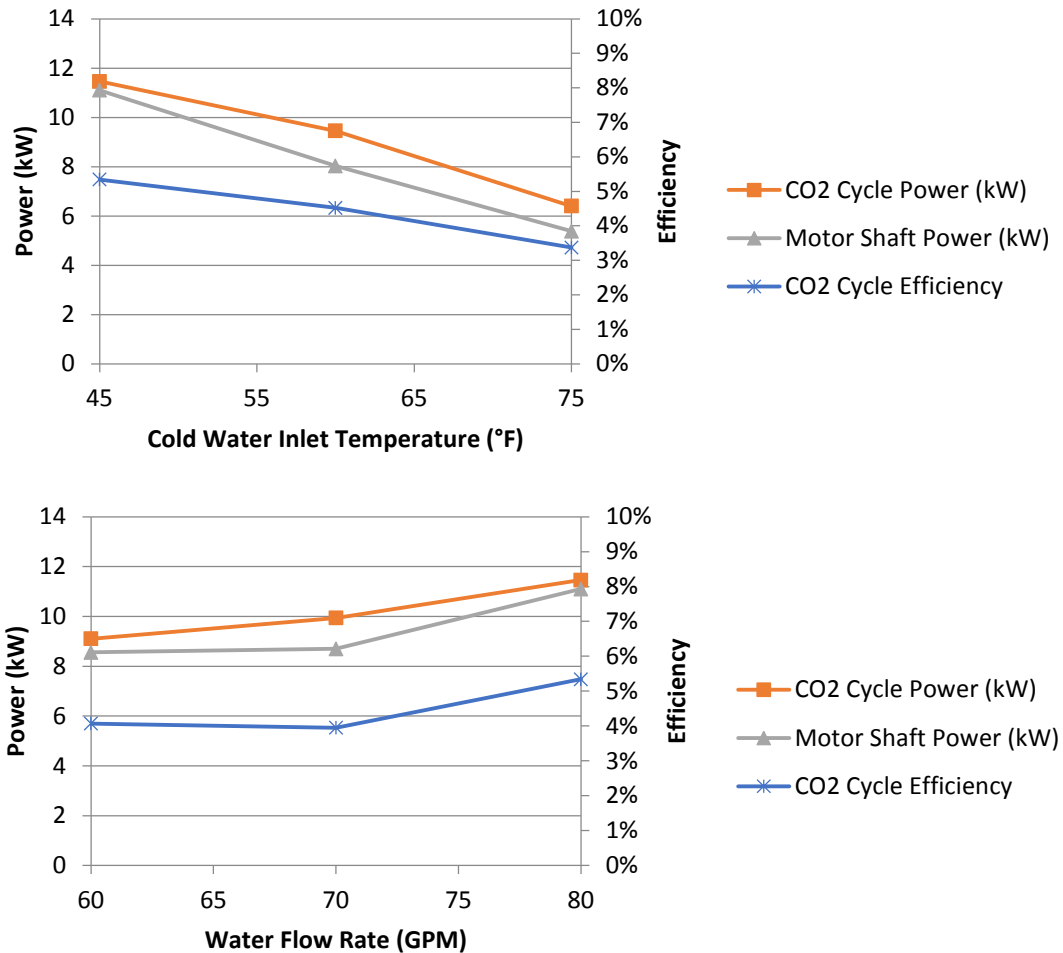


Figure 13. Effect on Power Output and Efficiency with Changes in Cold Water Temperature and Water Flow Rate for 190F Hot Water Temperature

The tests successfully demonstrated produced power from the engines at hot input temperatures ranging from 130°F to 190°F. This is the first prototype of this kind to demonstrate usable power from these ultra-low temperature heat sources. The goal of future development will be to improve cycle efficiencies and create behaviors that allow the engine to approach the Carnot limit. Improvements are being designed, specifically moving away from alternating hot and cold sources on the same heat exchanger, which should reduce exergetic losses and improve efficiencies. Further heat losses incurred

by heating and cooling the same mass of metals will also be reduced in future designs. Future engines that include the planned improvements will also allow for different fluids as hot and cold sources, since these sources will have different, dedicated heat exchangers.

REFERENCES

[1] Lemmon, E.W., Huber, M.L., McLinden, M.O. NIST Standard Reference Database 23: Reference Fluid Thermodynamic and Transport Properties-REFPROP, Version 9.1, National Institute of Standards and Technology, Standard Reference Data Program, Gaithersburg, 2013.

ACKNOWLEDGEMENTS

SwRI would like to thank Thermal Tech Holdings, LLC and PwrCor, Inc. for funding and supporting this research into an ultra-low temperature engine. Without their dedication and commitment to success, this effort would not have been possible.